Physics-Aware Bottleneck-First Target Coverage Scheduling for Solar-Powered Wireless Rechargeable Sensor Networks

Pei Xu[1], Su Wang[1], Huan-Chao Keh[2], Ssu-Chi Kuai[3], Diptendu Sinha Roy[4]*

[1] School of Artificial Intelligence and Big Data, Hefei University, China
[2] Department of Computer Science and Information Engineering, Tamkang University, Taiwan
[3] Department of Information Management, National Taipei University of Business, Taiwan
[4] Department of Computer Science and Engineering, National Institute of Technology Meghalaya, India
xupei@hfuu.edu.cn, ws030802@163.com, hckeh@mail.tku.edu.tw, sckuai@ntub.edu.tw, diptendu.sr@nitm.ac.in

Abstract

Long-term target coverage in solar-powered wireless rechargeable sensor networks (WRSNs) is fundamentally challenged by sensing uncertainty, weather-driven energy variability, and the strong coupling between adjustable sensing ranges and energy consumption. Existing approaches often rely on simplified sensing or harvesting models, which may lead to unstable schedules and degraded coverage at vulnerable targets.

This paper proposes Physics-aware Bottleneck-first Target Coverage Scheduling (PBTCS), a unified framework for sustainable target coverage in WRSNs under energy-neutral operation constraints. PBTCS integrates a physics-prior, interpretable day-ahead photovoltaic (PV) forecasting model to derive feasible and auditable energy budgets, and employs a budget-driven time partitioning mechanism to stabilize day-night operations. Based on the probabilistic sensing model, a bottleneck-first scheduling principle is introduced to explicitly prioritize the weakest space-time points, rather than optimizing average coverage metrics. To efficiently realize this objective under adjustable sensing radii, a closed-form marginal-gain decomposition and a budgeted dynamic programming scheme are developed for per-sensor schedule construction.

Extensive simulations using real PV and meteorological data demonstrate that PBTCS consistently outperforms state-of-the-art methods in surveillance quality, coverage fairness, and long-term network sustainability across different seasons and network scales.

Keywords: Wireless rechargeable sensor networks, Target coverage, Probabilistic sensing model, Energy-neutral scheduling

1 Introduction

Wireless sensor networks (WSNs) have become an indispensable infrastructure for a wide range of cyber-physical applications, including environmental monitoring, intruder detection, industrial inspection, and smart-city surveillance [1-2]. In these systems, coverage is a fundamental performance indicator because it directly reflects how reliably the physical world can be sensed over space and time. Depending on mission requirements, coverage problems are commonly categorized into area coverage, barrier coverage, and target coverage. Area coverage aims to monitor an entire region (e.g., farmland or a factory floor), barrier coverage focuses on detecting intruders crossing a protected boundary (e.g., borders, coastlines, and pipelines), while target coverage concentrates sensing resources on a designated set of points of interest (POIs), such as critical infrastructures, intersections, or key assets [3, 21]. This paper studies long-term target coverage, where the network must sustain reliable monitoring quality for all POIs over extended periods.

Despite extensive progress, achieving robust long-term target coverage remains challenging because practical deployments must simultaneously cope with sensing uncertainty and energy uncertainty. On the sensing side, the widely used Boolean sensing model (BSM) assumes perfect detection within a sensing radius and zero detection outside, which greatly simplifies analysis [27-28]. However, BSM ignores signal attenuation, shadowing, and environmental noise, and thus cannot capture the gradual decay of detection reliability with distance or the benefit of multi-sensor cooperation under noisy measurements [4]. On the energy side, conventional battery-powered WSNs inevitably suffer energy depletion, which leads to node failures, coverage holes, and even network partitioning [5-6]. In many scenarios, frequent battery replacement is costly or infeasible, motivating the development of wireless rechargeable sensor networks (WRSNs) that incorporate energy replenishment mechanisms. Among various recharge options, solar energy harvesting is particularly attractive due to its sustainability and ease of deployment, offering the potential for long-term operation when the network can maintain energy-neutral operation (ENO), i.e., consumption does not exceed harvested energy over time [8-9].

Recent hardware advances further allow sensors to adjust their sensing radii dynamically [10-11]. While adjustable radii provide valuable flexibility to strengthen monitoring quality for weak POIs, they also fundamentally

*Corresponding Author: Huan-Chao Keh; Email: hckeh@mail.tku.edu.tw
DOI: https://doi.org/10.70003/160792642026032702012

complicate system design. First, temporal supply-demand mismatch arises because solar energy is harvested mainly during daytime, whereas surveillance is typically required continuously, making nighttime operation difficult to guarantee without explicit planning for energy shifting across time [12-13]. Second, prediction uncertainty becomes a critical bottleneck: photovoltaic (PV) output depends on nonlinear meteorological drivers (e.g., irradiance, temperature, humidity, cloud cover, and wind), and inaccurate forecasts can produce unreliable energy budgets [30-33]. Importantly, forecast errors do not remain isolated--they propagate into downstream scheduling decisions, potentially causing energy-deficient operation and sudden coverage degradation. Third, scheduling complexity increases sharply under adjustable radii because sensing power typically scales super linearly with the radius (often quadratically) [24-26], creating strong energy heterogeneity among sensing modes. Consequently, the scheduler must carefully trade off surveillance quality and sustainability, and it becomes insufficient to optimize average performance without explicitly prioritizing the most vulnerable targets and time periods.

Existing literature has attempted to address parts of these challenges but often falls short in capturing the coupled physical realities of sensing and energy harvesting [14-17]. On the sensing side, BSM-based formulations may overestimate coverage quality and fail to differentiate between single-sensor and cooperative observations under realistic noise conditions [22-23]. On the energy side, many approaches adopt simplified harvesting assumptions (e.g., constant PV rates), which can be overly conservative or fundamentally inaccurate in volatile weather. Another line of research employs data-driven PV forecasting, including black-box deep learning predictors, which may achieve good average accuracy but usually provide limited interpretability and weak auditability for feasibility-critical scheduling. Some recent works (e.g., MSQBE) use similarity-based matching to estimate future PV power by retrieving historical days with similar meteorological conditions. While such methods reduce modeling burden, their precision may degrade under rapidly changing weather, leading to systematic mismatches between the derived energy budget and the actual operational demand. These limitations motivate a unified framework that (i) produces physically plausible, auditable day-ahead PV budgets and (ii) leverages them to construct bottleneck-aware schedules under probabilistic cooperative sensing.

To overcome the above limitations, we propose Physics-aware Bottleneck-first Target Coverage Scheduling (PBTCS), a new framework for long-term target coverage in solar-powered WRSNs with adjustable sensing radii. PBTCS adopts the Probabilistic Sensing Model (PSM) to quantify probabilistic detection reliability and cooperative sensing quality [7], and formulates a joint optimization over sensing radii and activation schedules under ENO constraints. The core principle of PBTCS is bottleneck-first optimization: since long-term surveillance quality is often dominated by a small subset of weak POIs (and corresponding vulnerable time periods), the scheduler should explicitly identify and reinforce these bottleneck space-time points, rather than merely improving aggregate metrics that may hide worst-case failures. Meanwhile, to make this bottleneck-first scheduling stable and feasible, PBTCS tightly couples physics-aware day-ahead PV forecasting with a budget-driven time discretization mechanism, ensuring that the derived schedule remains aligned with realistic energy availability.

The main contributions of this work are summarized as follows:

(1) Physics-prior interpretable and feasible day-ahead PV forecasting. We develop a lightweight forecasting model that combines a physical baseline (capturing irradiance-driven generation with temperature and wind-cooling effects) with an additive residual component. The forecast is explicitly constrained to a feasibility envelope (e.g., nonnegativity and rated-power limits) and supports term-level attribution, enabling auditable diagnosis of forecast deviations and reducing the risk that implausible estimates destabilize downstream scheduling.

(2) Budget-driven dynamic time partitioning for energy-neutral operation. Based on the day-ahead PV profile, PBTCS dynamically discretizes continuous time into slots and cycles whose parameters are derived from the predicted energy budget. This mechanism explicitly balances daytime harvesting and round-the-clock consumption, providing a principled bridge between physical energy availability and discrete scheduling decisions, especially for stabilizing nighttime operation under ENO constraints.

(3) Bottleneck-first budgeted scheduling under probabilistic cooperative sensing. We propose a bottleneck-first objective that prioritizes improving the cooperative detection probability at the weakest space-time points, and then enhances overall surveillance quality as a secondary goal. Under adjustable radii and ENO constraints, PBTCS constructs distributed schedules that jointly optimize sensing radius and activation slots, allocating limited energy to where it most effectively mitigates coverage vulnerabilities.

(4) Marginal-gain decomposition and efficient dynamic programming for per-sensor optimization. We derive a closed-form marginal contribution of activating a sensor with a given radius at a given slot to the cooperative detection probability, which converts the coupled cooperative-coverage optimization into a budgeted "slot selection'' problem. Building on this structure, we design an efficient dynamic programming recursion with schedule recovery, enabling each sensor's best-response schedule to be computed under controllable complexity and supporting scalable implementation.

The remainder of this paper is organized as follows. Section 2 reviews related work on probabilistic sensing, energy-harvesting scheduling, and target coverage in WRSNs. Section 3 introduces the system model and

formulates the bottleneck-first target coverage problem under ENO constraints. Section 4 presents the proposed PBTCS framework in detail. Section 5 evaluates the performance of PBTCS under diverse seasonal and network settings. Finally, Section 6 concludes the paper and discusses future research directions.

2 Related Work

In recent years, the target coverage problem in wireless sensor networks (WSNs) has attracted sustained attention due to its direct relevance to surveillance quality and service continuity in monitoring applications. Depending on the sensing capability and the energy supply model, existing studies can be broadly discussed from two complementary perspectives: (i) sensing-side modeling and controllability (e.g., fixed versus adjustable sensing radius), and (ii) energy-side sustainability (e.g., battery-powered versus rechargeable/energy-harvesting). Following the writing convention in the literature, we organize the most relevant studies into four classes: WSNs with fixed sensing radius sensors, WSNs with adjustable sensing radius sensors, WSNs with battery-powered sensors, and WSNs with rechargeable sensors (including solar-powered and hybrid energy-harvesting networks). This taxonomy also highlights the gap addressed by our Physics-aware Bottleneck-first Target Coverage Scheduling (PBTCS): jointly handling probabilistic sensing, weather-driven energy uncertainty, and bottleneck-first resource allocation under energy-neutral operation constraints.

2.1 WSNs With Fixed Sensing Radius Sensors

With fixed sensing radius sensors, the target coverage problem is comparatively easier to analyze, which has motivated a rich body of work on barrier/target coverage formulations, performance bounds, and tractable optimization heuristics. Study [1] investigated physical security in stealthy lattice WSNs and studied k-barrier coverage conditions under specific lattice topologies, providing insights into how deployment regularity affects barrier strength. Study [5] considered directional sensor networks and proposed a Discrete Army Ant Search Optimizer (DAASO) to improve target coverage under bound-constrained optimization, which is particularly useful when random deployment causes perception blind spots. To better match practical sensing behavior, several works adopt probabilistic sensing rather than deterministic binary detection. For example, Study [8] used the probabilistic sensing model (PSM) and investigated connected target coverage (CTC) with directional probabilistic sensors under an attenuation model; the resulting minimum-energy coverage problem was shown to be computationally challenging and was addressed via a transformation to a network flow formulation. Study [30] further explored barrier repair with mobile sensors under PSM: they introduced "safe cells" and barrier gaps, and then employed the Kuhn-Munkres (KM) assignment to dispatch mobile sensors with minimized movement cost. Beyond specific algorithms, surveys and overviews also emphasize that uncertainty-aware coverage modeling is critical when sensing and communication are affected by fading, shadowing, and environmental noise. Overall, fixed-radius designs provide clean analytical structures, yet they lack operational flexibility because sensing effort cannot be adapted to target importance or energy availability, which becomes a key limitation when the network must remain sustainable over long horizons.

2.2 WSNs With Adjustable Sensing Radius Sensors

To improve deployment flexibility and adapt sensing effort to mission demands, adjustable sensing radius sensors have been increasingly studied. A representative early formulation is Adjustable Range Set Covers (AR-SC) proposed by Study [6], where sensors with tunable ranges are organized into multiple set covers to extend the network lifetime. From an optimization viewpoint, Study [33] proposed the Neighborhood-based Estimation of Distribution Algorithm (NEDA) to maximize lifetime by selecting coverage schemes with specific radii and allocating activation time via a linear programming backbone. More closely related to bottleneck-aware coverage, Study [31] developed the Target Coverage Mechanism for Sensors with Adjustable Sensing Range (TCSAR) in wireless rechargeable sensor networks (WRSNs), where sensors are first selected based on their contribution to bottleneck points of interest (POIs), and then non-critical sensors reduce sensing radii to save energy while maintaining/improving the worst-case surveillance quality. These studies collectively demonstrate that radius control offers an effective "quality-energy" lever; however, it also introduces strong heterogeneity because sensing energy typically grows nonlinearly with the radius (often super-linear or quadratic with respect to range), making joint decisions on radius and duty-cycling significantly more complex than fixed-radius scheduling. Moreover, most adjustable-radius designs still require a principled way to align radius adaptation with time-varying energy budgets and to prioritize coverage improvements at the most vulnerable (bottleneck) targets under probabilistic sensing.

2.3 WSNs With Battery-Powered Sensors

In traditional battery-powered WSNs, energy depletion is the primary cause of coverage holes and network failure; hence, a large body of work focuses on maximizing lifetime under coverage and connectivity constraints. Study [29] presented a two-phase optimization framework for connected target coverage (CTC), using a multi-objective integer linear programming (ILP) model to form disjoint cover sets and a branch-and-bound procedure to optimize relay paths. Study [6] studied lifetime maximization with bounded relay-hop connectivity and developed an exact linear programming formulation together with scalable approximation techniques based on partitioning and shifting, thereby improving computational scalability while preserving coverage guarantees. Study [32] investigated synchronous placement of sensors and sinks and proposed a dual-population coevolutionary constrained multi-objective optimization algorithm (DCCMO) to balance

energy consumption and information effectiveness in structural monitoring scenarios. Despite these advances, battery-powered solutions fundamentally remain "finite-horizon'': once the initial energy is exhausted, node failures are inevitable, and coverage sustainability cannot be ensured without external recharging or harvesting mechanisms.

2.4 WSNs With Rechargeable Sensors

To overcome the finite-energy limitation, recent research has shifted toward WRSNs that exploit mobile charging or environmental energy harvesting (most notably solar energy). Study [18] proposed the Maximizing Cooperative Detection Probability (MCDP) algorithm for barrier coverage under PSM, aiming at perpetual lifetime by partitioning both timeline and region into space--time points and then scheduling sensors to improve cooperative detection, especially at bottleneck space-time points. For charger-assisted WRSNs, Study [3] introduced a reinforcement learning (RL)-based recharging strategy to guide a mobile charger via reward-and-penalty signals, optimizing the travel/charging trade-off. For purely solar-powered target coverage, Study [29] designed an interleaving cover-set scheduling mechanism to manage energy consumption and maintain coverage continuity across time. Study [8] considered complete target coverage with hybrid harvesting (e.g., radio-frequency (RF) plus solar) and formulated a mixed-integer linear programming (MILP) model to optimize the time allocation among harvesting, sensing, and communication. More broadly, energy-harvesting coverage has also been discussed through comprehensive surveys and systematizations, which highlight the coupling among stochastic harvesting, duty-cycling, and quality-of-service (QoS) coverage objectives. In addition, emerging architectures (e.g., aerial sensing/collection and the Internet of Drones) have been reviewed in the context of large-scale monitoring and integration with WSN/Internet of Things (IoT) infrastructures [17], suggesting that future coverage systems may incorporate heterogeneous platforms and mobility—yet the energy-neutral scheduling challenge remains central.

3 Assumption and Problem Statement

This section introduces the network environment, the probabilistic sensing model, and the charging–discharging model. Then, the problem statement and constraints are formulated.

3.1 Network Environment

We consider a solar-powered wireless rechargeable sensor network (WRSN) deployed in a two-dimensional monitored region $\Omega \subset \mathbb{R}^2$. Let $S = \{s_1, s, \ldots, s_n\}$ denote the set of sensor nodes and let $O = \{o_1, o_2, \ldots, o_n\}$ denote the set of monitoring targets (points of interest, POIs). A sink node is deployed to collect sensed data and coordinate network operations.

Each sensor is equipped with a photovoltaic (PV) energy-harvesting module and a rechargeable battery. Moreover, each sensor supports an adjustable sensing radius selected from a discrete candidate set $R = \{r^{(1)}, r^{(2)}, \ldots, r^{(L)}\}$ with $r^{(1)} < r^{(2)} < \ldots < r^{(L)}$. An illustrative deployment is shown in Figure 1, where red triangles represent targets, circles represent sensors with their sensing ranges, and the sink aggregates data through wireless communications.

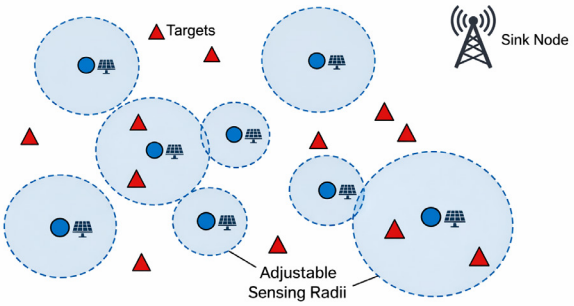

Figure 1. Example of considered WRSNs

3.2 Sensing Model

In this work, the *Probabilistic Sensing Model* (*PSM*) is adopted to capture sensing uncertainty caused by attenuation, shadowing, and environmental noise. The conceptual structure of the PSM is illustrated in Figure 2. Let $p(s_i, o_h)$ denote the instantaneous detection probability that sensor s_i detects the target o_h, and let $d(s_i, o_h)$ be their Euclidean distance. Under the PSM, $p(s_i, o_h)$ is modeled as a distance-dependent function:

$$p(s_i, o_h) = \begin{cases} 1, & d(s_i, o_h) \le r_g \\ \exp\left(-\lambda\left(d(s_i, o_h) - r_g\right)^{\zeta}\right), & r_g < d(s_i, o_h) \le r_m \\ 0, & d(s_i, o_h) > r_m \end{cases} \quad (1)$$

where r_g and r_m denote the guaranteed sensing radius and the maximum sensing radius, respectively, and $\lambda > 0$ and $\zeta > 0$ control the attenuation shape.

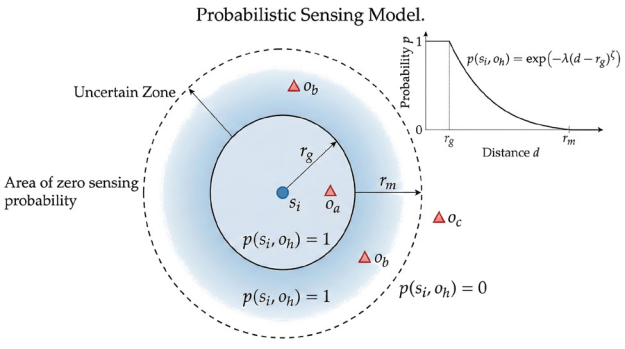

Figure 2. The probabilistic sensing model

For a point o_h, let $S(o_h)$ denote the set of active sensors that can cover o_h. The cooperative detection probability of these sensors at o_h is

$$p\left(S,o_h\right)=1-\prod_{s_i\in S\left(o_h\right)}\left(1-p(s_i,o_h)\right) \tag{2}$$

3.3 Charging and Discharging Model

In the considered WRSNs, each sensor is solar-powered and may operate in one of four states: *charging-and-sensing*, *charging-only*, *sensing-only*, and *sleeping*. Let $E_i^{\max}$ denote the battery capacity of sensor s_i. Let $e_i(r)$ denote the sensing energy consumption rate (power) when s_i operates with sensing radius $r\in\mathcal{R}$. Following the commonly used radius–power relationship, we model

$$e_i\left(r\right)=e_i\left(r^{(L)}\right)\left(\frac{r}{r^{(L)}}\right)^2 \tag{3}$$

where $r^{(L)}$ is the maximum sensing radius in R and $e_i(r^{(L)})$ is assumed known.

Time is divided into identical scheduling cycles, and each cycle is further discretized into M time slots of length τ. To simplify calculations, we assume that the relationship between the maximum sensing radius $r^{(L)}$ and any other sensing radius $r^{(j)}$ satisfies

$$\frac{r^{(L)}}{r^{(j)}}=\sqrt{L-j+1} \tag{4}$$

Let $T_i(r)$ denote the active sensing time of s_i in one cycle when operating with radius r under the same per-cycle sensing energy budget. Then,

$$T_i\left(r\right)=T_i\left(r^{(L)}\right)\cdot\frac{e_i\left(r^{(L)}\right)}{e_i\left(r\right)}=T_i\left(r^{(L)}\right)\left(\frac{r^{(L)}}{r}\right)^2 \tag{5}$$

which shows that the achievable active time is inversely proportional to the sensing energy rate.

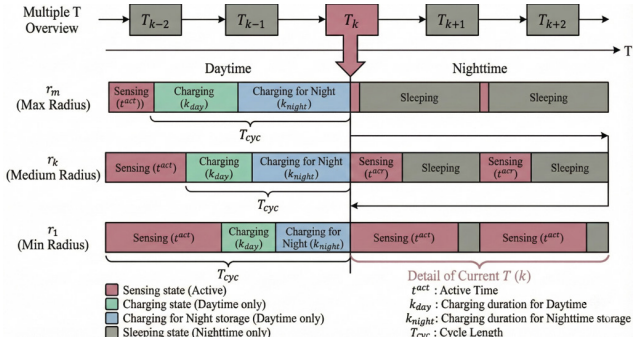

Figure 3. Example of charging and discharging model

Figure 3 illustrates the charging and discharging model within one scheduling cycle. Each sensor operates in four states: sensing-and-charging, charging-only, sensing-only, and sleeping. During daytime, sensing and energy harvesting can be performed simultaneously, while nighttime operation is restricted to sensing-only or sleeping. Under a fixed per-cycle energy budget, the achievable sensing duration depends on the selected sensing radius, where a smaller radius enables a longer active sensing time within the same cycle.

3.4 Problem Statement

The objective is to design a scheduling strategy that determines the sensing radius and the active slots for each sensor in every cycle so as to maximize the surveillance quality while satisfying the energy-neutral operation constraint. In target coverage applications, reliable surveillance requires that all targets be adequately monitored. As a result, the overall surveillance quality of a scheduling strategy is fundamentally constrained by the weakest-covered target. If any target experiences insufficient cooperative detection performance, the coverage objective is compromised regardless of how well other targets are monitored.

Accordingly, the surveillance quality of a scheduling strategy π is characterized by the cooperative detection performance of its weakest target. Let $o_h\in O$ denote a target. To ensure robustness over time, we further consider the temporal variation of cooperative sensing performance within a scheduling cycle. Each cycle is divided into M time slots indexed by $\{1, 2, \ldots, M\}$, and let $S(t)$ denote the set of active sensors at slot t. Under strategy π, the surveillance quality of target o_h over one cycle is therefore defined as the worst-case cooperative detection probability across all time slots, which is

$$U_h\left(\pi\right)=\min_{t\in\{1,\ldots,M\}}p\left(o_h,t\right) \tag{6}$$

Since multiple targets exist, the overall surveillance quality achieved by strategy π is determined by the weakest target among all targets, which is given by

$$U\left(\pi\right)=\min_{o_h\in O}U_h\left(\pi\right) \tag{7}$$

With this formulation, maximizing $U(\pi)$ guarantees that the cooperative detection probability of every target is improved in a worst-case sense over both space and time. Accordingly, the target coverage scheduling problem is formulated as

$$\max_{\pi}U\left(\pi\right) \tag{8}$$

which serves as the objective function of this paper. The objective function is subject to a set of constraints, which are specified as follows.

(1) State Constraint

Let $z_i^{cs}(t)$, $z_i^{c}(t)$, $z_i^{s}(t)$, and $z_i^{sl}(t)$ be binary variables indicating that sensor s_i is in charging-and-sensing, charging-only, sensing-only, or sleeping mode at slot t, respectively. Each sensor must stay in exactly one state at any slot:

$$z_i^{cs}(t)+z_i^{c}(t)+z_i^{s}(t)+z_i^{sl}(t)=1,\forall i,\forall t. \tag{9}$$

(2) Cycle-Working Constraint

To ensure that each sensor participates in surveillance tasks at least once per cycle, we impose

$$\sum_{t=1}^{M}(z_i^{cs}(t)+z_i^{s}(t))\geq 1,\forall i. \tag{10}$$

(3) Energy Balance Constraint

Let $P_i^{pv}(t)$ denote the harvested PV power of sensor s_i at slot t, and let $[t_s^{day}, t_e^{day}]$ denote the daytime interval within each cycle. Let $r_{i,t}\in R$ be the sensing radius selected by s_i at slot t. Denote the per-slot sensing energy rate as $e_i(r_{i,t})$ for $r_{i,t} > 0$. Over the planning horizon of N_{cyc} cycles, the harvested energy during daytime should balance the total sensing energy consumption:

$$\begin{aligned}&\sum_{j=1}^{N_{cyc}}\sum_{t\in\left[t_s^{day},t_e^{day}\right]}P_i^{pv}(t)\tau\ \geq\\&\sum_{j=1}^{N_{cyc}}\sum_{t=1}^{M}(z_i^{cs}(t)+z_i^{s}(t))e_i(r_{i,t})\tau,\forall i\ .\end{aligned} \tag{11}$$

where τ is the slot length.

Section 4 presents the proposed PBTCS algorithm, which aims to achieve the objective function in Exp. (7) while satisfying constraints Exps. (9)-(11).

4 The Proposed PBTCS Algorithm

We propose a novel target coverage algorithm, PBTCS, for WRSNs utilizing solar-powered sensors with adjustable sensing radii. The primary objective is to optimize the sensing radius and activation schedule of each sensor to maximize target surveillance quality while maintaining energy neutrality.

As shown in Figure 4, the PBTCS framework comprises three phases: time partitioning, detection probability calculation, and sensor scheduling. The first phase leverages physics-prior similarity-based calculations to forecast the next day's photovoltaic (PV) power based on historical meteorological data. Subsequently, continuous time is discretized into uniform slots and cycles, sized dynamically according to the predicted energy budget to balance acquisition and consumption. These slots and targets form a spatiotemporal grid for quality evaluation. The second phase quantifies the surveillance contribution of each sensor via detection probability. Finally, the scheduling phase identifies bottleneck spatiotemporal points and distributes tasks to maximize the collective surveillance quality.

4.1 Time Dividing Phase

This phase discretizes continuous time into uniform slots organized into cycles. This is because time is continuous, estimating the cooperative detection probability at every spatiotemporal point is intractable; thus, time is discretized into uniform slots for computable evaluation and scheduling. To ensure consistent surveillance quality, the sensor task schedule is identical within each slot of a cycle. Slot and cycle lengths are dynamically determined from the estimated harvesting potential and consumption rates. This process includes: 1) day-ahead PV forecasting via a similarity-based physics-prior model, and 2) computing slot and cycle lengths to balance the energy budget.

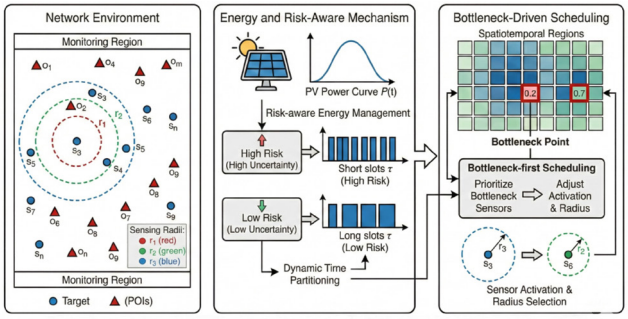

Figure 4. The overall framework of the proposed PBTCS

Step 1: Day-Ahead PV Power Forecasting via Physics-Prior Interpretable Additive Modeling

Day-ahead PV power forecasting provides a deterministic energy-input profile for energy-aware decision making over the next operating day. In many deployments, the forecaster must output a time-consistent full-day PV trajectory under limited computation and with clear interpretability, because the predicted profile is subsequently used to derive energy budgets and to diagnose forecast failures under meteorological shifts. In addition, when the forecast is directly consumed by downstream optimization, it is crucial to guarantee feasibility and provide auditable explanations; as formalized in Theorem 1, the proposed physics-prior additive formulation ensures an always-feasible prediction through interval projection and offers exact term-level attribution with a bounded deviation from the physical baseline. Deep learning models have been widely adopted for PV forecasting [19-20], but they are often less transparent in a model-intrinsic sense and may require extra mechanisms to support stable deployment and failure-mode interpretability.

To meet these requirements, we propose a physics-prior, interpretable additive forecasting framework that outputs both a full-day PV profile and factor-wise attributions. The method couples a lightweight physical baseline (encoding sign-known effects of irradiance,

temperature, cloud cover, and wind cooling) with an additive residual learner that captures systematic deviations driven by weather dynamics and site conditions.

Input and physics-prior baseline. The next day is discretized into M slots with centers $t = 1, \ldots, M$. For each slot, the available covariates are summarized as

$$x_t = \left(GHI_t, T_t^{amb}, RH_t, CC_t, WS_t, terr\right), t = 1, \cdots, M \quad (12)$$

where GHI is global horizontal irradiance, T amb is ambient temperature, RH is relative humidity, CC is cloud cover, WS is wind speed, and $terr$ denotes a terrain class that absorbs persistent shading/albedo and microclimate effects. A physics-prior baseline is computed as

$$P_{phy}(t) = P_{rated} \cdot k(terr) \cdot \left(\frac{GHI_t}{GHI_{ref}}\right) \cdot \left[1 - \gamma\left(T_t^{cell} - T_{ref}\right)\right]_+ \quad (13)$$

where P_{rated} is the plant capacity (or an equivalent normalization), $k(terr) \in (0, 1]$ is a terrain-dependent derating factor, γ is the temperature coefficient, and $[\cdot]_+ = max(\cdot, 0)$. The cell temperature is approximated by

$$T_t^{cell} = T_t^{amb} + \eta \cdot GHI_t - \nu \cdot WS_t \quad (14)$$

with η, $\nu > 0$ capturing irradiance-driven heating and wind-driven convective cooling. This baseline enforces physically consistent trends: the output increases with irradiance, is penalized by excessive cell temperature, and is naturally suppressed during low-irradiance intervals.

Explainable residual learning (additive structure). The baseline in Exps. (12) and (13) is intentionally lightweight and cannot fully represent transient cloud attenuation, aerosol variability, or systematic forecast bias. We therefore learn an additive residual correction:

$$\Delta(t) = b + \sum_{j=1}^{d} f_j(z_t, j) + \sum_{(j,k)\in\mathcal{L}} f_{jk}(z_{t,j}, z_{t,k}) \quad (15)$$

where $z_{t,j}$ are selected features (e.g., CC_t, RH_t, WS_t, irradiance trends, and terrain indicators), $f_j(\cdot)$ are one-dimensional shape functions, and $f_{jk}(\cdot,\cdot)$ are a small number of optional pairwise interactions ($|I|$ is kept small to preserve interpretability). The functions can be instantiated by constrained splines or explainable boosting in an additive form, and domain-consistent constraints may be imposed when appropriate (e.g., monotone non-increasing response with respect to cloud cover and monotone non-decreasing response with respect to irradiance-related factors).

The final day-ahead prediction is obtained by a physically consistent projection:

$$\hat{P}(t) = \prod_{[0, P_{rated}]}\left(P_{phy}(t) + \Delta(t)\right), t = 1, \cdots, M \quad (16)$$

where $\prod_{[0, Prated]}$ clips the result into the feasible range.

Training and interpretability outputs. Given historical pairs $\{(x_t, P(t))\}$, the additive residual is fitted by minimizing a robust regularized objective

$$\min_{\{f_j, f_{jk}\}} \sum_{t\in T_{tr}} \rho\left(P(t) - P_{phy}(t) - \Delta(t)\right) + \lambda\left(\sum_{j=1}^{d} \Omega(f_j) + \sum_{(j,k)\in L} \Omega(f_{jk})\right) \quad (17)$$

where $\rho(\cdot)$ is a Huber (or quantile) loss and $\Omega(\cdot)$ penalizes roughness/complexity. After training, the forecaster outputs not only $\hat{P}(t)$ but also slot-wise, term-level attributions

$$Attr_j(t) = f_j(z_t, j), Attr_{jk}(t) = f_{jk}(z_t, j, z_t, k) \quad (18)$$

which enables direct inspection of which factors drive the forecast at each slot.

Theorem 1 (Feasibility and Exact Attribution of Physics-Prior Interpretable Additive Forecasting)

Let $P_{phy}(t)$ be defined by Exp. (13), and let $\Delta(t)$ follow the additive structure Exp. (15). Define $\hat{P}(t)$ by Exp. (16). Assume each learned component is bounded: $|f_j(\cdot)| \le B_j$ and $|f_{jk}(\cdot,\cdot)| \le B_{jk}$. Then:

1) **(Physical feasibility)** For all t, $\hat{P}(t) \in [0, P_{rated}]$.

2) **(Exact additive attribution)** For all t, the pre-projection admits the decomposition

$$P_{phy}(t) + \Delta(t) = P_{phy}(t) + b + \sum_{j=1}^{d} Attr_j(t) + \sum_{(j,k)\in\mathcal{L}} Attr_{jk}(t) \quad (19)$$

3) **(Controlled deviation from the baseline)** The deviation from the projected baseline is uniformly bounded:

$$\left|\hat{P}(t) - \prod_{[0,P_{rated}]}\left(P_{phy}(t)\right)\right| \le |b| + \sum_{j=1}^{d} B_j + \sum_{(j,k)\in\mathcal{L}} B_{jk} \quad (20)$$

Proof.

(1) By definition, the projection $\prod_{[0, Prated]}(\cdot)$ maps any real number into $[0, P_{rated}]$; thus $\hat{P}(t) \in [0, P_{rated}]$ for all t.

(2) From Exp. (15) and the attribution definitions, we have

$$\Delta(t) = b + \sum_{j=1}^{d} Attr_j(t) + \sum_{(j,k)\in\mathcal{L}} Attr_{jk}(t) \quad (21)$$

Substituting into $P_{phy}(t) + \Delta(t)$ gives the stated decomposition.

(3) Projection onto an interval is non-expansive, i.e., $|\prod(u)-\prod(v)| \le |u-v|$. Let $u = P_{phy}(t) + \Delta(t)$ and $v = P_{phy}(t)$. Then

$$\left|\hat{P}(t)-\prod_{[0,P_{rated}]}\left(P_{phy}(t)\right)\right| \le |\Delta(t)| \le |b| + \sum_{j=1}^{d}\left|f_j(z_t,j)\right| + \sum_{(j,k)\in\mathcal{L}}\left|f_{jk}(z_t,j,z_t,k)\right| \tag{22}$$

Applying $|f_j| \le B_j$ and $|f_{jk}| \le B_{jk}$ yields the bound.

□

Step 2: Calculating the Length of One Time Slot and Cycle

Based on the estimated PV power, this step determines the slot and cycle durations to enforce energy neutrality across day and night operations. Let t_{day}^{start} and t_{day}^{end} define the daylight period. The total expected energy E_{exp}^{total} is obtained by integrating the forecast function. Since solar harvesting is restricted to daytime, energy budgets for daytime (E_{day}) and nighttime (E_{night}) consumption must satisfy:

$$E_{day} + E_{night} \le E_{exp}^{total} \tag{23}$$

We define the time slot length τ as the active duration of a sensor operating with the maximum sensing radius. Given a unit energy budget per cycle E_{unit} and the maximum power consumption rate $e_i(L)$, the slot length is:

$$\tau = \frac{E_{unit}}{e_i(L)} \tag{24}$$

Cycle length depends on the charging time required to offset consumption. Let k_{day} and k_{night} represent the number of slots allocated for energy accumulation during the day to support daytime and nighttime operations, respectively. With an average charging rate P_{avg}^{char}, the daytime charging slots k_{day} must satisfy $k_{day}\,\tau\,P_{avg}^{char} = E_{unit}$, yielding:

$$k_{day} = \frac{E_{unit}}{\tau P_{avg}^{char}} \tag{25}$$

Consequently, the total energy stored during the day for nighttime use is determined by the number of daytime cycles N_{cyc}^{day}. For the night period of duration T_{night}, the required number of charging slots k_{night} is derived to ensure total nighttime consumption $N_{cyc}^{night}\,E_{unit}$ is covered by the stored energy. Finally, the total length of one cycle is:

$$T_{cyc} = \left(k_{day} + k_{night} + 1\right)\tau \tag{26}$$

This temporal structure ensures continuous operation. The subsequent phase calculates the detection probabilities for target coverage.

4.2 Detection Probability Calculation Phase

This phase quantifies the surveillance quality by calculating the detection probability of each sensor relative to each target. Leveraging the sensing model defined in Section 3, the detection probability $p(s_i, o_h)$ depends on the Euclidean distance $d(s_i, o_h)$ and the sensing radius r_i.

For a single sensor s_i, the probability is derived via Exp. (1). If multiple sensors cover a target simultaneously, the cooperative surveillance quality of sensors to this target can be calculated by applying Exp. (2).

Figure 5 illustrates this process. As shown, target o_1 lies outside any sensing range, resulting in $p(o_1) = 0$. Target o_2 is monitored solely by s_1, with probability derived directly from Exp. (1), we have

$$p(s_1,o_2) = \begin{cases} 1, & d(s_1,o_2) \le r_g \\ \exp\left(-\lambda\left(d(s_i,o_h)-r_g\right)^{\zeta}\right), & r_g < d(s_1,o_2) \le r_m \end{cases} \tag{27}$$

Furthermore, target o_3 is jointly covered by $S(o_3) = \{s_1, s_2, s_3\}$. The resulting cooperative probability is:

$$p(S,o_3) = 1 - \prod_{s_i \in S(o_3)} (1 - p(s_i,o_3)) \tag{28}$$

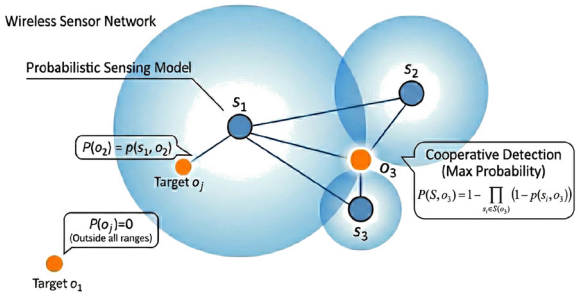

Figure 5. Example of calculating the detection probability

The following phase utilizes these values to identify bottleneck space-time points (those with the weakest coverage) and prioritizes scheduling sensors with the highest contribution to these vulnerabilities.

4.3 Sensor Scheduling Phase

This phase optimizes the activation schedule—specifically sensing radii and active time slots—for all sensors to maximize network-wide surveillance quality. The process executes iteratively in two steps: 1) identifying the bottleneck space-time point characterized by the lowest cooperative detection probability, and 2) scheduling the sensor with the highest potential contribution to mitigate this vulnerability.

Step 1: Identifying the Bottleneck Space–Time Point

Recall that continuous time is discretized into slots, forming a set of space–time points. A point (o_h, t_k) represents target o_h during time slot t_k. In the distributed PBTCS framework, each sensor s_i maintains a Local Monitoring Region (LMR), denoted as $R_{LMR}(s_i)$, containing targets within its maximum sensing range. Extending this temporally, the local monitoring space–time region $R^{ST}_{LMR}(s_i)$ encompasses all points (o_h, t_k) where $o_h \in R_{LMR}(s_i)$ and t_k represents a slot within the cycle:

$$R^{ST}_{LMR}(s_i) = \left\{(o_h, t_k) \mid o_h \in R_{LMR}(s_i), t_k \in T_{cyc}\right\} \quad (29)$$

Let $p(o_h, t_k)$ denote the cooperative detection probability for point (o_h, t_k), calculated via the aggregation of active sensors $S_{h,k}$, which is the set of active sensors that can cover o_h at t_k. Sensor s_i identifies its local bottleneck point (o_b, t_b), which can be identified by the following expression:

$$(o_b, t_b) = arg \min_{(o_h, t_k) \in R^{ST}_{LMR}(s_i)} p(o_h, t_k) \quad (30)$$

To execute this, s_i maintains two matrices: the local surveillance quality matrix M_Q and the local schedule matrix M_S. M_S tracks the scheduling status of neighboring sensors (defined as those within communication range), while M_Q stores the resulting cooperative probabilities for points in $R^{ST}_{LMR}(s_i)$.

Upon receiving broadcasted schedules from neighbours, s_i updates M_S, recomputes the elements of M_Q using the cooperative probability formula, and identifies the local bottleneck via Exp. (30). The bottleneck point (o_b, t_b) serves as the optimization target for the subsequent scheduling step.

Step 2: Constructing the Best Schedule for Each Sensor (Bottleneck-Aware Budgeted DP)

This step constructs, for each sensor, an energy-feasible working schedule that prioritizes improving the cooperative sensing quality at the current bottleneck space-time point while maintaining a structured and verifiable optimization criterion. Consider one planning cycle discretized into T_{cyc} time slots $t_k \in \{1, \ldots, M\}$, and a discrete radius set R for sensor s_i. A per-sensor schedule is denoted by $\mathcal{X}_i = (r_i, \mathcal{S}_i)$, where $r_i \in R$ is the selected radius for the cycle and $\mathcal{S}_i \subseteq \{1, ..., M\}$ is the set of activated slots (sleeping otherwise). Equivalently, define a per-slot radius sequence $r_{i,t} = r$ if $t \in \mathcal{S}_i$, and $r_{i,t} = 0$ otherwise.

Cooperative detection update (*neighbours fixed*). Let $p_i(o_h, r_i) \in [0,1]$ denote the single-sensor detection probability of sensor s_i on target o_h when using radius r_i. With neighbor schedules fixed, define the cooperative detection probability excluding sensor i at space-time point (o_h, t_k) as $\hat{p}^{-i}(o_h, t_k) = 1 - \prod_{s_j \in S_{old,h,k}, j \neq i} (1 - p_j(o_h, t_k))$, where $S_{old,h,k}$ is the set of sensors currently active at (o_h, t_k) excluding s_i. Then, for any candidate schedule $\mathcal{X}_i$, the updated cooperative detection probability is

$$p(o_h, t_k; \chi_i) = 1 - \left(1 - \hat{p}^{-i}(o_h, t_k)\right)\left(1 - p_i(o_h, r_i)\right) \quad (31)$$

Bottleneck-first lexicographic objective. Recall (o_b, t_b) is the identified bottleneck space-time point in the current iteration, and let x_i^{old} be the incumbent schedule of sensor s_i. We define the bottleneck improvement $\Delta_{bot}(x_i) = p(o_b, t_b; \mathcal{X}_i) - \hat{p}^{-i}(o_b, t_b)$ as the primary objective and the aggregated local improvement over an evaluation target set O_i as the secondary objective $\Delta_{local}(x_i) = \sum_{o_h \in R^{ST}_{LMR}(s_i)} \sum_{t_k \in T_{cyc}} [p(o_h, t_k; \mathcal{X}_i) - \hat{p}^{-i}(o_h, t_k)]$. The schedule of sensor s_i is selected by lexicographic maximization:

$$\chi_i^* = arg \max_{x_i \in \chi_i} \langle \Delta_{bot}(\mathrm{X}_i), \Delta_{local}(\mathrm{X}_i) \rangle \quad (32)$$

This criterion enforces "bottleneck-first" improvement, while using a deterministic, quality-consistent tie-breaker when multiple schedules yield the same bottleneck gain.

Slot-wise marginal contribution (*closed form*). To avoid enumerating all $(r_i, \mathcal{S}_i)$ combinations, we evaluate the marginal gain of activating sensor i at a given slot t under fixed neighbors. Let $p(o_h, t_k; r_i)$ denote the cooperative detection when sensor i is active at slot t_k with radius r_i, and let $p(o_h, t_k; r_i = 0)$ denote the cooperative detection when it sleeps. Their difference admits the closed-form expression

$$\begin{aligned} \Delta p(o_h, t_k \mid i, t_k, r_i) &\triangleq p(o_h, t_k; r_i) - p(o_h, t_k; r_i = 0) \\ &= p_i(o_h; r_i) \Pi_{s_j \in S_{old,h,k}, j \neq i} \left(1 - p_i(o_h, t_k; r_j)\right) \end{aligned} \quad (33)$$

Based on $\Delta p(\cdot)$, for a fixed radius r_i, define a per-slot value pair: $u_1(t; r_i) = \Delta p(o_b, t_b \mid i, t, r_i) \cdot 1\{t = t_b\}$ (bottleneck gain) and $u_2(t; r_i) = \sum_{o_h \in R_{LMR}(s_i)} \Delta p(o_h, t_k \mid i, t, r_i)$(overall local gain at slot t).

Energy-neutral budget and switching constraint. The energy-neutral operation constraint induces a radius-dependent activation budget $K_i(r) \in \mathbb{Z}_+$, i.e., $|S_i| \leq K_i(r)$. To suppress excessive switching and capture practical duty-cycling latency, we further enforce a minimum separation $\delta \geq 0$: if $t, t' \in S_i$ and $t < t'$, then $t' - t \geq \delta + 1$. Accordingly, define $prev(t) = max\{t' \leq t - (\delta + 1)\}$ (or 0 if none exists).

Budgeted DP synthesis. For each $r_i \in R$, schedule synthesis reduces to selecting $\mathcal{S}_i \subseteq \{1, \ldots, M\}$ that maximizes the lexicographic sum of (u_1, u_2) subject to the budget and separation constraints. Let $DP[t, k; r_i]$ be the best lexicographic pair achievable using slots up to t with at most k activations under radius r_i. The recurrence is

$$DP[t, k; r_i] = \max_{lex} \begin{Bmatrix} DP[T-1, k], \\ DP[prev(t), k-1] \\ + (u_1(t; r_i), u_2(t; r_i)) \end{Bmatrix} \quad (34)$$

with boundaries $DP[0, k] = (0,0)$ and $DP[t, 0] = (0,0)$. The optimal activation set $S_i^*(r_i)$ is recovered by backtracking from $DP[M, K_i(r)]$, yielding $\mathcal{X}_i(r_i) = (r, S_i^*(r_i))$; finally, $\mathcal{X}_i^*$ is obtained by lexicographic comparison over $r_i \in R$.

Theorem 2 (Lexicographic Dominance of the Proposed DP over MSQBE).

Consider a single iteration where (i) neighbor schedules are fixed, (ii) the feasible set of schedules for sensor s_i is identical for both methods (i.e., the same radius set R, the same ENO-induced budget $|\mathcal{S}_i| \le K_i(r_i)$, and the same minimum separation δ), and (iii) the cooperative detection update follows Exp. (31) . Define

$$\begin{aligned} F_1(\chi_i) &\triangleq p(o_b, t_b; \chi_i) - p\left(o_b, t_b; \chi_i^{\text{old}}\right), \\ F_2(\chi_i) &\triangleq \sum_{t_k \in T_{cyc}} \sum_{o_h} p(o_h, t_k; \chi_i) \\ &\quad - p\left(o_h, t_k; \chi_i^{old}\right) \end{aligned} \tag{35}$$

and let $\mathcal{X}_i^*$ be the schedule returned by the proposed DP that lexicographically maximizes (F_1, F_2) as in Exp. (32). Let $\mathcal{X}_i^{MSQBE}$ be the schedule returned by MSQBE, which first maximizes the bottleneck benefit (i.e., the bottleneck improvement) and then resolves ties using a variance-based dispersion criterion on the updated local quality matrix. Then the following statements hold:

1. (Lexicographic optimality) For any feasible schedule $\mathcal{X}_i$,

$$\left(F_1\left(\chi_i^\star\right), F_2\left(\chi_i^\star\right)\right) \succeq_{lex} \left(F_1(\chi_i), F_2(\chi_i)\right) \tag{36}$$

2. (Weak dominance over MSQBE) In particular,

$$\begin{aligned} &F_1\left(\chi_i^\star\right) \ge F_1\left(\chi_i^{MSQBE}\right), \\ &\text{and if } F_1\left(\chi_i^\star\right) = F_1\left(\chi_i^{MSQBE}\right) \\ &\text{then } F_2\left(\chi_i^\star\right) \ge F_2\left(\chi_i^{MSQBE}\right) \end{aligned} \tag{37}$$

3. (Strict improvement is realizable) There exist feasible instances such that

$$F_1\left(\chi_i^\star\right) = F_1\left(\chi_i^{MSQBE}\right) \text{ but } F_2\left(\chi_i^\star\right) > F_2\left(\chi_i^{MSQBE}\right) \tag{38}$$

Proof.

(1) Lexicographic optimality. Fix a radius $r_i \in R$. Under fixed neighbours, the slot-wise marginal improvement $\Delta p(o_h, t_k | i, t_k, r_i)$ is given by Exp. (33), hence both the bottleneck gain and the aggregated gain are additively decomposable across selected slots via $u_1(t_k; r_i)$ and $u_2(t_k; r_i)$. The feasibility constraints are captured solely by (i) a cardinality budget $k \le K_i(r_i)$ and (ii) the separation constraint encoded by $prev(t_k)$. Therefore, the problem admits optimal substructure: the optimal lexicographic value achievable up to slot t_k with budget k is obtained by either skipping slot t or selecting slot t and combining it with the optimal solution up to $prev(t_k)$ with budget $k-1$, which is exactly the recurrence Exp. (34). By induction on t, $DP[t, k; r_i]$ equals the lexicographically maximal sum of (u_1, u_2) over all feasible activation sets within $\{1, \ldots, M\}$. Consequently, $DP[M, K_i(r_i); r_i]$ yields the lexicographically optimal schedule for the fixed radius r. Taking the lexicographic maximum over $r_i \in R$. completes the proof of global lexicographic optimality for $\mathcal{X}_i^*$ with respect to (F_1, F_2), establishing statement (1).

(2) Weak dominance over MSQBE. Since $\mathcal{X}_i^{MSQBE}$ is feasible by assumption, it lies in the feasible set optimized by the DP. Applying statement (1) to $\mathcal{X}_i^{MSQBE}$ immediately yields $(F_1(\mathcal{X}_i^*), F_2(\mathcal{X}_i^*)) \succeq_{lex} (F_1(\mathcal{X}_i^{MSQBE}), F_2(\mathcal{X}_i^{MSQBE}))$, which implies statement (2).

(3) Strict improvement is realizable. MSQBE resolves ties among schedules with equal bottleneck benefit using a variance-based dispersion criterion on the updated local quality matrix. Such a tie-breaker is generally not equivalent to maximizing F_2. Hence, one can construct an instance with two feasible schedules $\mathcal{X}^{(a)}$ and $\mathcal{X}^{(b)}$ such that both activate at t_b and cover g_b, giving equal bottleneck improvement $F_1(\mathcal{X}^{(a)}) = F_2(\mathcal{X}^{(b)})$, while $\mathcal{X}^{(a)}$ additionally activates at some $t' > t_b$ that yields strictly positive aggregated gains on a subset of targets $o_h \in R_{LMR}(s_i)$, implying $F_2(\mathcal{X}^{(a)}) > F_2(\mathcal{X}^{(b)})$ by the nonnegativity of Exp. (33). Meanwhile, by choosing neighbor baselines $\hat{p}^{-i}$ and local target composition appropriately, the extra gains under $\mathcal{X}^{(a)}$ can be made more uneven, leading to a larger variance than $\mathcal{X}^{(b)}$, so MSQBE selects $\mathcal{X}^{(b)}$ whereas the proposed DP selects $\mathcal{X}^{(a)}$. Therefore, F_1 ties but F_2 is strictly larger under $\mathcal{X}_i^*$, proving statement (3).

□

5 Simulation

This section evaluates the performance of the proposed PBTCS algorithm by benchmarking it against two representative target-coverage schemes for solar-powered WRSNs, namely MSQBE and TCSAR. MSQBE is designed for WRSNs with adjustable sensing radii and aims to maximize the surveillance quality under energy-neutral operation by explicitly modeling probabilistic sensing and the charging–discharging dynamics; it further incorporates a lightweight PV-power evaluation based on historical-day similarity to guide day-ahead energy budgeting. In contrast, TCSAR focuses on adjustable-radius target coverage and improves the weakest monitored points through iterative radius adaptation (starting from a high-radius configuration and then refining radii to enhance the minimum coverage quality), while its energy harvesting process is abstracted by a simplified perpetual operation model that assumes a known, constant charging rate during daytime and no harvesting at night, rather than performing day-/hour-level PV prediction. The following presents the simulation environment and results.

5.1 Simulation Environment

Table 1 lists the simulation parameters of the

experimental study. All simulations are conducted in MATLAB R2023b over a 450 m × 450 m monitoring region with sensors and targets randomly deployed. The number of sensors varies from 200 to 1000, while the number of targets ranges from 10 to 50. Each sensor has a sensing radius between 12 m and 36 m and a communication radius of 72 m, with a 4 m guaranteed sensing region for each target. The battery capacity of each sensor is 1500 J, and the maximum power consumption rate is limited to 72 J/h. Time-varying harvested energy is modeled using real photovoltaic and meteorological data from the Public PV/Meteorological dataset, enabling realistic evaluation under seasonal energy dynamics.

Table 1. Simulation parameters

Parameter	Value
Simulation tool	MATLAB R2023b
Monitoring region	450m×450m
Number of sensors	200-1000
Number of targets	10-50
Minimum sensing radius	12m
Maximum sensing radius	36m
Communication radius	72m
Battery capacity of each sensor	1500 Joule
The radius of guaranteed sensing region	4m
Maximum power consumption rate	72 Joules/hour
PV power and meteorological data	Dataset from DKA solar center
Deployment strategy	Randomly

5.2 Experiment Results

Figure 6(a)–Figure 6(d) present the surveillance quality results in Spring, Summer, Autumn, and Winter, respectively. The three-dimensional bar charts compare PBTCS, MSQBE, and TCSAR in terms of Surveillance Quality under different combinations of Number of Targets and Number of Sensors. Overall, increasing the number of sensors from 200 to 1000 consistently improves surveillance quality for all three methods, indicating that denser sensor deployments enhance cooperative coverage capability. In contrast, for a fixed sensor configuration, increasing the number of targets leads to a noticeable performance degradation, reflecting the coverage dilution effect induced by higher sensing loads.

Across all four seasonal scenarios, a stable performance ranking is observed, namely PBTCS outperforms MSQBE, which in turn outperforms TCSAR. Among the three methods, PBTCS achieves the highest surveillance quality under most configurations and exhibits particularly strong advantages in bottleneck scenarios characterized by a large number of targets and a limited number of sensors. This demonstrates its superior robustness and efficiency in resource allocation. In the Summer scenario, the overall surveillance quality of all methods shifts upward due to more favorable energy conditions; nevertheless, the relative advantage of PBTCS remains pronounced, indicating that the additional resources are effectively translated into uniform, target-wide performance gains rather than improvements limited to easy-to-cover configurations.

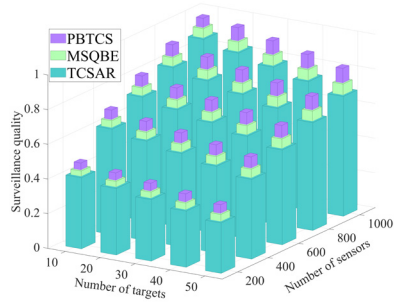

(a) Spring

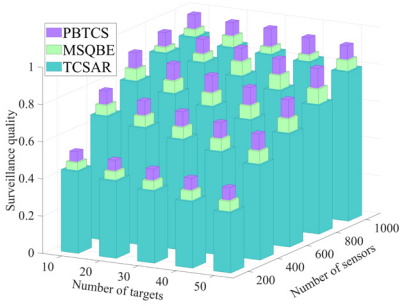

(b) Summer

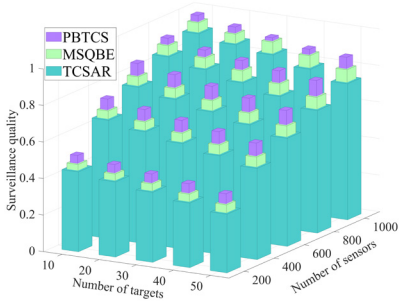

(c) Autumn

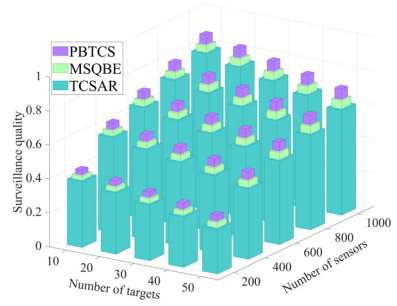

(d) Winter

Figure 6. Surveillance quality comparison of PBTCS, MSQBE, and TCSAR under different numbers of targets and deployed sensors across seasons

In comparison, performance degradation becomes more evident in the Autumn and Winter scenarios, especially under energy-constrained conditions. In these challenging regimes, TCSAR experiences the most severe decline in surveillance quality, while MSQBE shows moderate robustness. Notably, PBTCS continues to maintain

relatively high surveillance quality even under reduced energy availability and increased task load, highlighting its strong adaptability to adverse operating conditions.

Overall, the results demonstrate that PBTCS consistently delivers superior stability and scalability across different seasonal environments and network scales. Its ability to mitigate performance degradation in high-load and resource-constrained scenarios validates its effectiveness for cooperative surveillance in complex and dynamic sensing environments.

Figure 7(a)-Figure 7(d) report the distribution of cooperative detection probability across all targets under four randomly selected days in spring, summer, autumn, and winter, respectively. In each subplot, the x-axis enumerates the selected days, and each day contains three grouped boxplots corresponding to PBTCS, MSQBE, and TCSAR. Each box summarizes the cooperative detection probabilities of 50 targets on that day: the central line indicates the median, the box edges denote the 25th and 75th percentiles, and the whiskers represent the non-outlier range (with isolated markers indicating outliers). The three background bands ("Excellent/Good/Poor") provide a qualitative stratification of coverage quality, allowing an immediate visual inspection of whether the target-wise probabilities concentrate in high-quality regions.

As shown in Figure 7(a) (Spring) and Figure 7(c) (Autumn), PBTCS consistently yields boxplots with higher medians and, more importantly, compressed interquartile ranges, indicating that most targets are maintained at a uniformly high cooperative sensing probability instead of exhibiting large target-to-target disparities. By contrast, MSQBE shows a moderate reduction in dispersion relative to TCSAR but still presents noticeably lower lower-quartiles on several days, implying that a subset of targets experiences degraded cooperative sensing. TCSAR exhibits the widest boxes and longer lower whiskers, reflecting a stronger imbalance where certain targets receive insufficient cooperative sensing support.

The seasonal effect is most evident when comparing Figure 7(b) (Summer) with Figure 7(d) (Winter). In Summer, all methods benefit from higher harvested energy, hence the overall distributions shift upward; nevertheless, PBTCS remains the most concentrated and stays predominantly within the "Excellent/Good" bands, showing that the additional energy is translated into broad, target-wide gains rather than improvements limited to a few easy-to-cover targets. In Winter, due to reduced PV availability and tighter ENO constraints, all three methods experience a downward shift and more pronounced tails. Even in this challenging regime, PBTCS preserves the highest lower-quartiles and the smallest dispersion among the three baselines, demonstrating superior robustness in maintaining coverage fairness under energy scarcity.

These results align with the design rationale of PBTCS. By combining a physics-aware day-ahead PV profile with a bottleneck-first scheduling principle, PBTCS explicitly prioritizes the weakest spatiotemporal coverage conditions and allocates sensing effort to lift the worst-served targets. Consequently, the improvement is manifested not only in higher central tendency (median/mean) but also in a systematically reduced spread, which is the key signature of fairness-oriented cooperative sensing. In contrast, approaches that are less bottleneck-aware or less energy-consistent tend to exhibit higher variance across targets, leading to visible lower tails in the boxplots and a larger fraction of targets falling into the "Poor" band on low-energy days.

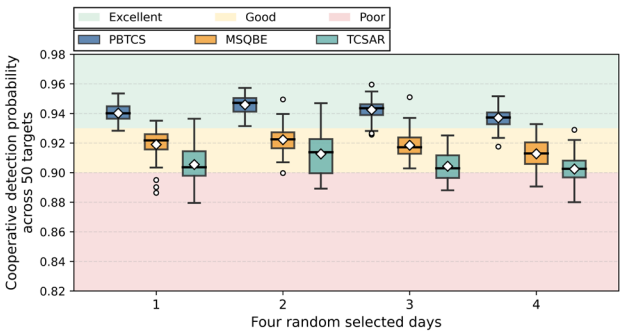

(a) Spring

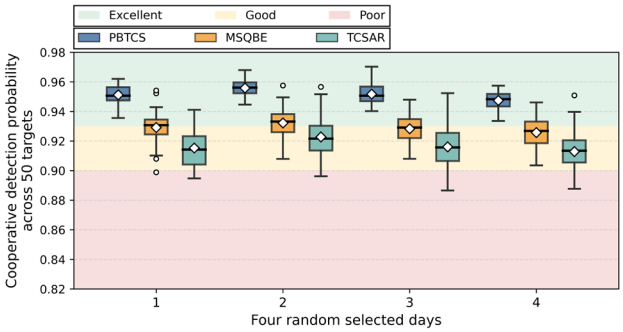

(b) Summer

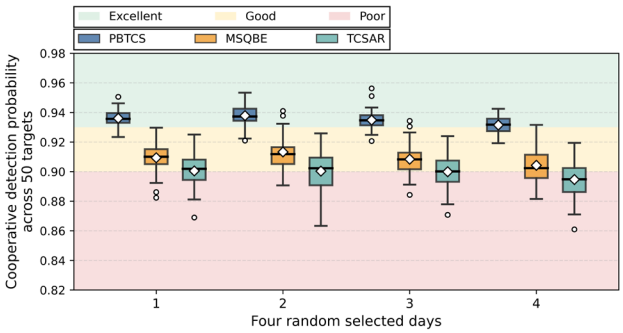

(c) Autumn

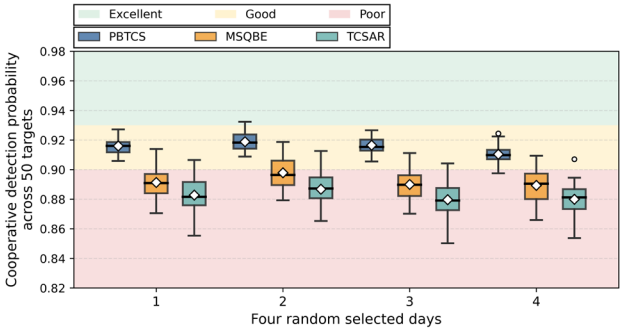

(d) Winter

Figure 7. Cooperative detection probability distribution comparison of PBTCS, MSQBE, and TCSAR across seasons

To evaluate energy sustainability and the effectiveness with which harvested solar energy is utilized under different scheduling strategies, we introduce the solar energy utilization ratio (SEUR), defined as

$$SEUR = \frac{ADE}{ASE} \times 100\%$$

where ADE denotes the actual daily energy consumption induced by the scheduling policy, including sensing, communication, and duty-cycling overheads, and ASE denotes the actual daily solar energy harvested by the photovoltaic (PV) system. Intuitively, SEUR≈100% indicates that the algorithm is well calibrated to the energy-neutral operation (ENO) budget and is able to fully exploit the available solar energy without accumulating long-term energy deficits; SEUR<100% implies an overly conservative scheduling strategy that underutilizes harvestable energy, thereby sacrificing potential sensing or surveillance capability; conversely, SEUR > 100% indicates that energy expenditure exceeds the realized energy harvest, leading to an energy deficit that accumulates as battery depletion and consequently increases the risk of node failures.

Figure 8 presents the day-wise SEUR over a 10-day horizon under four seasonal conditions, where each bar represents the network-level mean SEUR averaged across all nodes, and the error bars capture the dispersion across nodes and repeated trials. First, PBTCS remains tightly concentrated around the 100% baseline across all seasons, suggesting that its physics-aware day-ahead PV handling, together with the bottleneck-first budget mechanism, yields a well-calibrated energy plan that is neither overly conservative nor overly aggressive. Second, MSQBE typically exhibits SEUR values systematically above 100% with moderate variance, indicating weaker energy calibration along its prediction–scheduling pipeline and a tendency to overspend; this behavior becomes more pronounced in seasons with larger PV fluctuations, which is consistent with the higher dead-node ratios observed in long-horizon experiments. Third, TCSAR, which does not explicitly perform PV forecasting and instead relies on a simplified constant charging-rate assumption, shows the largest deviation from 100% and the widest error bars, reflecting pronounced inter-node imbalance and frequent budget mismatches; this behavior is also aligned with its substantially higher dead-node ratios over time. Finally, the seasonal ordering of SEUR aligns with PV availability: overall, SEUR is closest to 100% in summer and becomes most challenging in winter, where all methods exhibit larger deviations and higher dispersion; moreover, autumn consistently outperforms spring, consistent with the higher average PV power assumed in autumn.

Overall, these results demonstrate that PBTCS can maintain a stable and near energy-neutral level of solar energy utilization under seasonal PV variability, thereby achieving stronger energy sustainability and system reliability.

To further validate the impact of the energy utilization analysis on long-term system operation, we analyze the evolution of the dead sensor ratio over extended time horizons. Figure 9(a)-Figure 9(d) compare the evolution of the dead sensor ratio over a 60-day operation horizon in Spring, Summer, Autumn, and Winter, respectively. The dead sensor ratio is defined as the percentage of sensors whose residual energy drops below the operational threshold and thus can no longer participate in sensing and cooperation. All methods start from a near-zero dead ratio, while their curves gradually diverge as energy deficits accumulate and the ENO constraint becomes harder to satisfy.

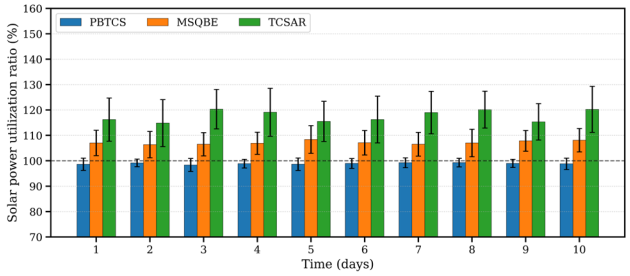

(a) Spring

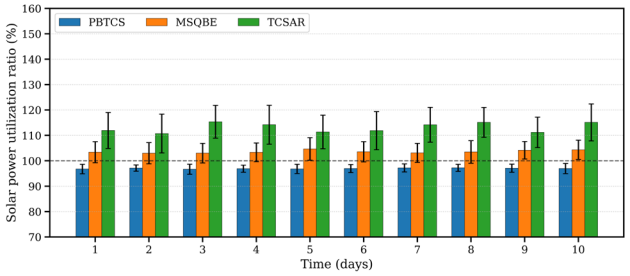

(b) Summer

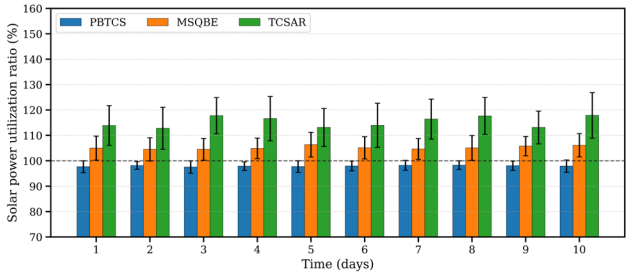

(c) Autumn

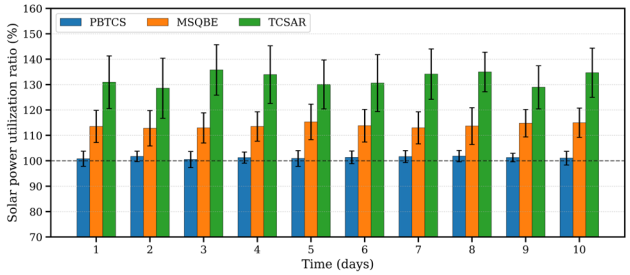

(d) Winter

Figure 8. Seasonal comparison of solar energy utilization ratio (SEUR) for PBTCS, MSQBE, and TCSAR

Across all seasons, PBTCS consistently exhibits the lowest death ratio and the slowest growth rate. In Figure

9(a), the advantage becomes pronounced after the first 2-3 weeks: PBTCS increases smoothly and remains around 10% at day 60, whereas MSQBE and TCSAR rise much faster and reach roughly 26% and 34%, respectively. Similar trends are observed in Figure 9(b) and Figure 9(d), where PBTCS preserves a single-digit terminal death ratio (about 5%-6%), while MSQBE stabilizes at a noticeably higher level (about 11%-13%) and TCSAR suffers the most severe node attrition (about 23%-24%). Figure 9(c) corresponds to a comparatively energy-favorable season where all curves are lower; nevertheless, PBTCS still maintains the smallest death ratio (about 4%-5% at day 60), outperforming MSQBE (about 9%) and TCSAR (about 15%). Overall, PBTCS reduces the long-term dead-node fraction by a clear margin against both baselines and, more importantly, delays the onset of rapid node failures.

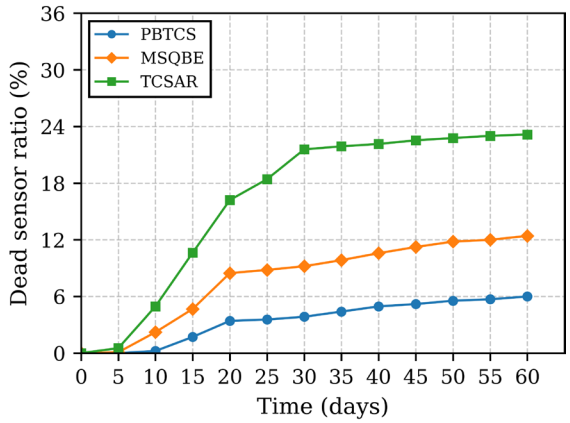

(a) Spring

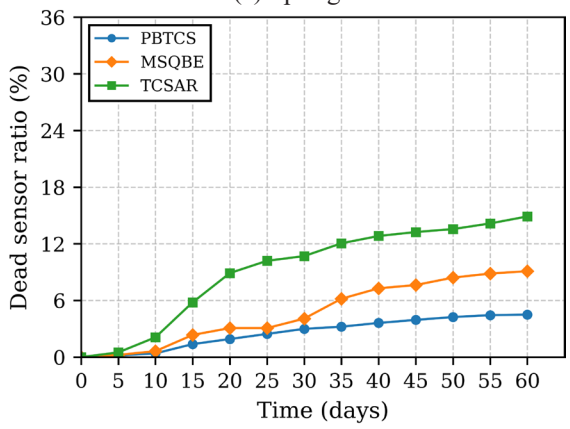

(b) Summer

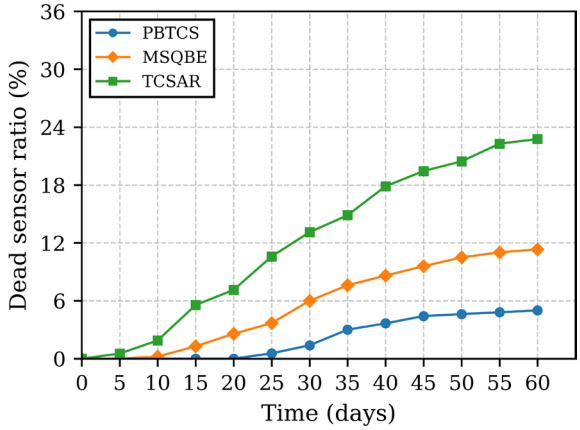

(c) Autumn

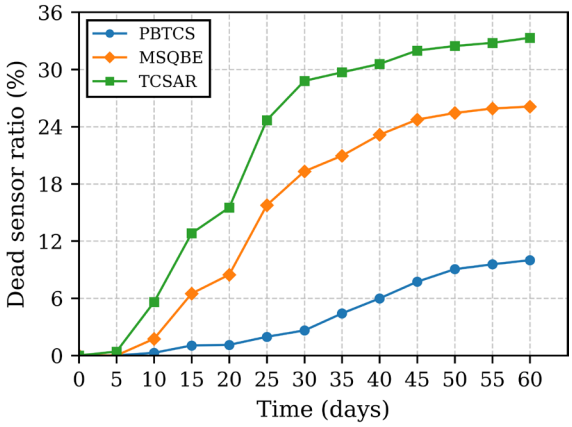

(d) Winter

Figure 9. Evolution of dead sensor ratio for PBTCS, MSQBE, and TCSAR across seasons

The above behaviors can be explained by the design of PBTCS. By leveraging a physics-aware day-ahead PV profile, PBTCS avoids overly optimistic energy assumptions and prevents aggressive early sensing that would otherwise deplete batteries and trigger cascaded node deaths. Meanwhile, the bottleneck-first scheduling explicitly allocates limited energy to the most critical spatiotemporal points, mitigating the tendency of heuristic schedules to over-serve locally easy regions and under-protect weak points. As a result, PBTCS achieves a more sustainable energy trajectory, which is reflected in both a lower terminal death ratio and a consistently flatter growth curve. The seasonal differences are also consistent with PV availability: in energy-scarce or high-variability seasons, the death ratios increase more rapidly for all schemes, and the robustness of PBTCS becomes more salient.

6 Conclusion

This paper introduces an innovative target coverage algorithm for Wireless Rechargeable Sensor Networks (WRSNs), referred to as PBTCS, which utilizes adjustable sensing radius sensors. The aim is to optimize surveillance quality while maintaining a balance between energy consumption and acquisition to ensure the network's longevity. To achieve this, the proposed PBTCS framework integrates a physics-prior model for forecasting photovoltaic (PV) power, enabling the division of the monitored region into multiple grids and time slots. These grids form space-time points that ensure a steady energy supply for each sensor during the operational cycle, including a reserve for nighttime operations. By identifying critical bottleneck points, PBTCS prioritizes coverage at the weakest space-time locations, constructing an optimal task schedule that allocates energy efficiently while maximizing the detection quality. Experimental results demonstrate that PBTCS outperforms existing algorithms in terms of surveillance quality, especially in scenarios with varying energy dynamics. Future work will extend this framework to incorporate additional factors in target coverage, including different types of sensors in heterogeneous WRSNs and varying coverage requirements.

Acknowledgment

This work was supported in part by an industry-sponsored research project under Grant 902/22050124126, and in part by an industry-sponsored research project under Grant 902/22050124063.

References

[1] Z. Liu, G. Jiang, W. Jia, T. Wang, Y. Wu, Critical Density for K-Coverage Under Border Effects in Camera Sensor Networks With Irregular Obstacles Existence, *IEEE Internet of Things Journal*, Vol. 11, No. 4, pp. 6426-6437, February, 2024.
https://doi.org/10.1109/JIOT.2023.3311466

[2] Y. Shao, Q. Wang, X. Lu, Z. Wang, E. Zhao, S. Fang, J. Chen, L. Kong, K. Z. Ghafoor, AutoBar: Automatic Barrier Coverage Formation for Danger Keep Out Applications in Smart City, *Sensors*, Vol. 23, No. 18, Article No. 7787, September, 2023.
https://doi.org/10.3390/s23187787

[3] Manju, S. Singh, S. Kumar, A. Nayyar, F. Al-Turjman, L. Mostarda, Proficient QoS-Based Target Coverage Problem in Wireless Sensor Networks, *IEEE Access*, Vol. 8, pp. 74315-74325, May, 2020.
https://doi.org/10.1109/ACCESS.2020.2986493

[4] J. Guo, Y. Sun, T. Liu, Y. Li, T. Fei, An Optimization Coverage Strategy for Wireless Sensor Network Nodes Based on Path Loss and False Alarm Probability, *Sensors*, Vol. 25, No. 2, Article No. 396, January, 2025.
https://doi.org/10.3390/s25020396

[5] Y. D. Yao, Q. Wen, Y. P. Cui, B. Z. Zhao, Discrete Army Ant Search Optimizer-Based Target Coverage Enhancement in Directional Sensor Networks, *IEEE Sensors Letters*, Vol. 6, No. 4, pp. 1-4, April, 2022.
https://doi.org/10.1109/LSENS.2022.3158274

[6] M. Cardei, J. Wu, M. Lu, M. O. Pervaiz, Maximum Network Lifetime in Wireless Sensor Networks With Adjustable Sensing Ranges, *IEEE International Conference on Wireless and Mobile Computing, Networking and Communications*, Montreal, QC, Canada, 2005, pp. 438-445.
https://doi.org/10.1109/WIMOB.2005.1512935

[7] M. A. Jamshed, K. Ali, Q. H. Abbasi, M. A. Imran, M. Ur-Rehman, Challenges, Applications, and Future of Wireless Sensors in Internet of Things: A Review, *IEEE Sensors Journal*, Vol. 22, No. 6, pp. 5482-5494, March, 2022.
https://doi.org/10.1109/JSEN.2022.3148128

[8] C. Li, K. W. Chin, C. Yang, Complete Target Coverage in Radio Frequency and Solar-Powered Sensor Networks, *IEEE Systems Journal*, Vol. 15, No. 3, pp. 3609-3619, September, 2021.
https://doi.org/10.1109/JSYST.2020.2997300

[9] P. Xu, X. Wang, C. Y. Chang, Y. Li, D. S. Roy, JMLA: Joint Monitoring Quality and Network Lifetime for Range-Adjustable Sensors in WRSNs, *IEEE Sensors Journal*, Vol. 24, No. 20, pp. 33522-33543, October, 2024.
https://doi.org/10.1109/JSEN.2024.3451521

[10] X. Xu, Z. Dai, A. Shan, T. Gu, Connected Target ε-Probability Coverage in WSNs With Directional Probabilistic Sensors, *IEEE Systems Journal*, Vol. 14, No. 3, pp. 3399-3409, September, 2020.
https://doi.org/10.1109/JSYST.2019.2939178

[11] J. Akram, H. S. Munawar, A. Z. Kouzani, M. A. P. Mahmud, Using Adaptive Sensors for Optimised Target Coverage in Wireless Sensor Networks, *Sensors*, Vol. 22, No. 3, Article No. 1083, February, 2022.
https://doi.org/10.3390/s22031083

[12] C. Zhang, Y. Li, P. Xu, C. Y. Chang, D. S. Roy, Dynamic Probabilistic Sensing for Enhanced Target Coverage in WRSNs, *IEEE Sensors Journal*, Vol. 24, No. 16, pp. 26699-26715, August, 2024.
https://doi.org/10.1109/JSEN.2024.3421656

[13] P. Xu, Y. Li, C. Y. Chang, C. H. Kuo, D. S. Roy, Dynamic Weather-Adaptive Enhanced Barrier Coverage with Adjustable-Range Sensors for WRSNs, *Journal of Internet Technology*, Vol. 26, No. 4, pp. 523-545, July, 2025.
https://doi.org/10.70003/160792642025072604011

[14] W. H. Liao, B. Dande, C. Y. Chang, D. S. Roy, MMQT: Maximizing the Monitoring Quality for Targets Based on Probabilistic Sensing Model in Rechargeable Wireless Sensor Networks, *IEEE Access*, Vol. 8, pp. 77073-77088, May, 2020.
https://doi.org/10.1109/ACCESS.2020.2989199

[15] R. Jia, H. Zhang, Wireless Sensor Network (WSN) Model Targeting Energy Efficient Wireless Sensor Networks Node Coverage, *IEEE Access*, Vol. 12, pp. 27596-27610, February, 2024.
https://doi.org/10.1109/ACCESS.2024.3365511

[16] P. S. Bharathi, R. Pavithra, Modified Bron-Kerbosch-Based Sensor Deployment Algorithm for Target Coverage in Wireless Sensor Networks, *IEEE Access*, Vol. 13, pp. 95692-95705, June, 2025.
https://doi.org/10.1109/ACCESS.2025.3575245

[17] L. Abualigah, A. Diabat, P. Sumari, A. H. Gandomi, Applications, Deployments, and Integration of Internet of Drones (IoD): A Review, *IEEE Sensors Journal*, Vol. 21, No. 22, pp. 25532-25546, November, 2021.
https://doi.org/10.1109/JSEN.2021.3114266

[18] P. Xu, J. Wu, C. Y. Chang, C. Shang, D. S. Roy, MCDP: Maximizing Cooperative Detection Probability for Barrier Coverage in Rechargeable Wireless Sensor Networks, *IEEE Sensors Journal*, Vol. 21, No. 5, pp. 7080-7092, March, 2021.
https://doi.org/10.1109/JSEN.2020.3043456

[19] S. M. Miraftabzadeh, M. Longo, High-Resolution PV Power Prediction Model Based on the Deep Learning and Attention Mechanism, *Sustainable Energy, Grids and Networks*, Vol. 34, Article No. 101025, June, 2023.
https://doi.org/10.1016/j.segan.2023.101025

[20] S. Al-Dahidi, H. Alahmer, B. Rinchi, A. Bani-Abdullah, M. Alrbai, O. Ayadi, L. Al-Ghussain, Multistep PV Power Forecasting Using Deep Learning Models and the Reptile Search Algorithm, *Results in Engineering*, Vol. 27, Article No. 106265, September, 2025.
https://doi.org/10.1016/j.rineng.2025.106265

[21] R. Pavithra, D. Arivudainambi, Coverage-Aware Sensor Deployment and Scheduling in Target-Based Wireless Sensor Network, *Wireless Personal Communications*, Vol. 130, No. 1, pp. 421-448, May, 2023.
https://doi.org/10.1007/s11277-023-10292-9

[22] Q. Zhao, C. Li, D. Zhu, C. Xie, Coverage Optimization of Wireless Sensor Networks Using Combinations of PSO and Chaos Optimization, *Electronics*, Vol. 11, No. 6, Article No. 853, March, 2022.
https://doi.org/10.3390/electronics11060853

[23] P. Anusuya, C. N. Vanitha, J. Cho, S. V. Easwaramoorthy, A comprehensive review of sensor node deployment

strategies for maximized coverage and energy efficiency in wireless sensor networks, *PeerJ Computer Science*, Vol. 10, Article No. e2407, November, 2024.
https://doi.org/10.7717/peerj-cs.2407

[24] A. J. Bakht, H. Motameni, H. Mohamadi, A learning automata-based algorithm for solving the target k-coverage problem in directional sensor networks with adjustable sensing ranges, *Physical Communication*, Vol. 42, Article No. 101156, October, 2020.
https://doi.org/10.1016/j.phycom.2020.101156

[25] B. Khalifa, A. M. Khedr, Z. Al Aghbari, A Coverage Maintenance Algorithm for Mobile WSNs With Adjustable Sensing Range, *IEEE Sensors Journal*, Vol. 20, No. 3, pp. 1582-1591, February, 2020.
https://doi.org/10.1109/JSEN.2019.2946623

[26] A. Qarehkhani, M. Golsorkhtabaramiri, H. Mohamadi, M. Y. Tabari, Solving target coverage problem in directional sensor networks with ability to adjust sensing range using continuous learning automata, *Journal of Intelligent & Fuzzy Systems*, Vol. 41, No. 6, pp. 6831-6844, December, 2021.
https://doi.org/10.3233/JIFS-210759

[27] Y. T. Chin, W. D. Jiang, H. C. Chang, W. H. Liao, LFP: A Stable and Efficient Local Interpretation Method for Deep Neural Networks, *IEEE International Conference on Consumer Electronics–Taiwan*, Kaohsiung, Taiwan, 2025, pp. 501-502.
https://doi.org/10.1109/ICCE-Taiwan66881.2025.11207975

[28] X. Bao, Y. Jiang, L. Han, X. Xu, H. Zhu, Distributed dynamic scheduling algorithm of target coverage for wireless sensor networks with hybrid energy harvesting system, *Scientific Reports*, Vol. 14, Article No. 27931, November, 2024.
https://doi.org/10.1038/s41598-024-78671-1

[29] D. K. Sah, A. Hazra, N. Mazumdar, A. C. S. Rao, T. Amgoth, An Efficient Scheduling Approach for Target Coverage in Solar Powered Internet of Things, *IEEE Transactions on Sustainable Computing*, Vol. 10, No. 5, pp. 1043-1055, September-October, 2025.
https://doi.org/10.1109/TSUSC.2025.3578433

[30] P. Si, J. Ma, F. Tao, Z. Fu, L. Shu, Energy-Efficient Barrier Coverage With Probabilistic Sensors in Wireless Sensor Networks, *IEEE Sensors Journal*, Vol. 20, No. 10, pp. 5624-5633, May, 2020.
https://doi.org/10.1109/JSEN.2020.2970435

[31] Q. Zhang, C. Y. Chang, Z. Dong, D. S. Roy, TCSAR: Target Coverage Mechanism for Sensors With Adjustable Sensing Range in WRSNs, *IEEE Sensors Journal*, Vol. 22, No. 4, pp. 3756-3765, February, 2022.
https://doi.org/10.1109/JSEN.2021.3139731

[32] Q. Yu, C. Yang, G. Dai, L. Peng, X. Chen, Synchronous Wireless Sensor and Sink Placement Method Using Dual-Population Co-evolutionary Constrained Multi-objective Optimization Algorithm, *IEEE Transactions on Industrial Informatics*, Vol. 19, No. 6, pp. 7561-7571, June, 2023.
https://doi.org/10.1109/TII.2022.3211853

[33] Z. G. Chen, Y. Lin, Y. J. Gong, Z. H. Zhan, J. Zhang, Maximizing Lifetime of Range-Adjustable Wireless Sensor Networks: A Neighborhood-Based Estimation of Distribution Algorithm, *IEEE Transactions on Cybernetics*, Vol. 51, No. 11, pp. 5433-5444, November, 2021.
https://doi.org/10.1109/TCYB.2020.2977858

Biographies

Pei Xu received the Ph.D. degree in Computer Science and Technology from Anhui University, Hefei, China, in 2020. He is currently a Lecturer with the School of Artificial Intelligence and Big Data, Hefei University, Hefei, China. His current research interests include smart sensing technology, the Internet of Things.

Su Wang received the B.S. degree in Network Engineering from Anhui Institute of Information Technology, Wuhu, China, in 2024. She is currently pursuing the M.S. degree with the School of Artificial Intelligence and Big Data, Hefei University, Hefei, China. Her research interests include wireless sensor networks, the Internet of Things.

Huan-Chao Keh received his M.S. and Ph.D. in Computer Science from Oregon State University. He is a full professor in the Department of Computer Science and Information Engineering at Tamkang University, Taiwan, and has served as its President since 2018. His interests include IoT, AI, and clinical medical information systems.

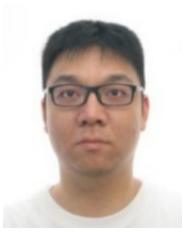

Ssu-Chi Kuai received his Ph.D. in Computer Science and Engineering from Tatung University, Taipei, Taiwan. He is an Assistant Professor in the Department of Information Management, National Taipei University of Business. His interests include WSNs, IoT, SDN, cloud computing, and generative AI/LLM applications.

Diptendu Sinha Roy received his Ph.D. from Birla Institute of Technology Mesra, India, in 2010. He is an Associate Professor at National Institute of Technology Meghalaya since 2017. His research interests include software reliability, distributed/cloud computing, IoT, and AI/ML for smart systems applications. IEEE Computer Society member.